CCS Chemistry

RESEARCH ARTICLE

Received: Sept. 12, 2023 | Accepted: Nov. 20, 2023 | Published: Dec. 19, 2023

Covalent Organic Framework with Predesigned Single-Ion Traps for Highly Efficient Palladium Recovery from Wastes

Yinghui Xie[1], Qiuyu Rong[1], Caimei Wen[1], Xiaolu Liu[1], Mengjie Hao[1], Zhongshan Chen[1], Hui Yang[1]*, Geoffrey I. N. Waterhouse[2], Shengqian Ma[3]* & Xiangke Wang[1]*

[1]*College of Environmental Science and Engineering, North China Electric Power University, Beijing 102206,* [2]*School of Chemical Sciences, The University of Auckland, Auckland 1142,* [3]*Department of Chemistry, University of North Texas, Denton, Texas 76201*

**Corresponding authors: h.yang@ncepu.edu.cn; shengqian.ma@unt.edu; xkwang@ncepu.edu.cn*

Cite this: *CCS Chem.* **2024**, 6, 1908–1919
DOI: 10.31635/ccschem.023.202303404

The recovery of palladium from waste streams is of importance for metal recycling and environmental remediation. Herein, we present a "single-ion trap" strategy for efficiently recovering Pd(II) from super-acidic solutions and laboratory wastes. This was realized by rational design and synthesis of an antiparallel stacked covalent organic framework (ACOF) with hydrazine-carbonyl sites and pyridine sites for cooperative Pd(II) capture. The single-ion traps provided Lewis base sites with a high Pd(II) binding affinity, enabling the trapping of Pd(II) ions under a wide range of conditions. The developed ACOF-1 adsorbent demonstrated fast kinetics, excellent selectivity, and a high adsorption capacity of 412.9 ± 14.2 mg/g for Pd(II) in a 3M HNO_3 solution. When applied in a packed column, ACOF-1 dynamically captured Pd(II) from 3M HNO_3 solutions or laboratory wastes containing trace amounts of palladium and many other metals, realizing extraction efficiencies of 232.9 and 320.9 mg/g, respectively. Detailed experimental and theoretical studies revealed that the single-ion traps offered exceptionally strong binding of Pd(II) under both acidic and high ionic strength conditions, enabling selective adsorptive behavior not accessible using traditional adsorbents. Importantly, the general design strategy reported here could be used to create porous adsorbents for the capture of other precious metals.

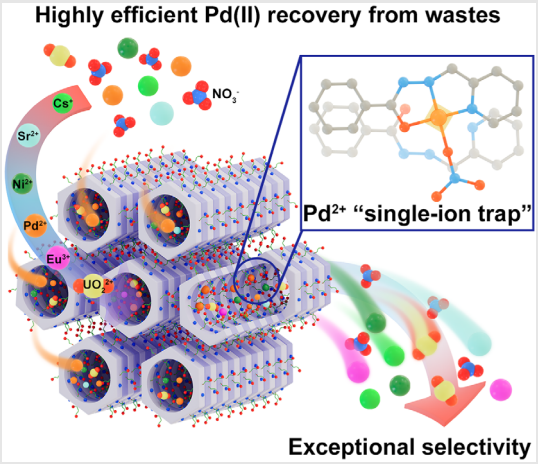

Keywords: antiparallel stacking, covalent organic frameworks, binding affinity, selective adsorption, Pd(II) recovery

DOI: 10.31635/ccschem.023.202303404
Citation: *CCS Chem.* **2024**, 6, 1908–1919
Link to VoR: https://doi.org/10.31635/ccschem.023.202303404

Introduction

As one of the most important precious metals, palladium finds widespread use in catalysis,[1-3] electronic devices,[4-6] corrosion resistance alloys,[7] and medicine.[8,9] Pd-based catalysts started to be used in organic synthesis more than one hundred years ago, with market demand for Pd increasing rapidly in recent years. Due to its low natural abundance, the market price of palladium reached an extremely high price of $3099/ounce in 2022, reflecting growing global demand and consumption.[10] To offset the supply-demand imbalance, the processing of secondary sources of Pd is necessary such as the recovery of Pd from spent catalysts,[11,12] high-level liquid nuclear waste (HLLW),[13,14] or scrap electronics.[15] In addition, if Pd-wastes are not treated properly, they can cause serious environmental pollution. Therefore, developing techniques for the selective recognition and recovery of such metal from waste has become a top priority. However, Pd recovery from palladium-containing scrap and waste is very challenging owing to the extreme conditions in which the Pd(II) and Pd(IV) ions separations must be performed, including (1) solutions where the concentration of palladium is low such as solutions obtained by dissolving Pd metal or Pd alloys in acid; (2) coexistence of other metal ions or high ionic strength environments; (3) strongly acidic and complex components in an acidic solution or HLLW; (4) Pd ions complexed by organic ligands as found in homogeneous catalysts and laboratory wastes, increasing the complexity of Pd extraction.

A number of methods, such as aluminum reduction[16] or bioreduction,[17,18] have been developed for the separation and recovery of palladium from strongly acidic solutions. However, the highly oxidizing nature of nitric acid hinders Pd(II)/Pd(IV) reduction, reducing the recovery efficiency and increasing the cost. Therefore, improved extraction methods need to be found for palladium recovery from highly acidic solutions. Recently, adsorption-based recovery using regenerable adsorbents has shown promise in terms of cost, practicality, and sustainability.

Various adsorbent materials such as porous carbon,[19] reduced graphene oxide,[20] titanium dioxide,[15] silica,[21-23] biomaterials,[17] carbon nitride,[24] organic polymers,[11,25-30] metal–organic frameworks (MOFs),[31-34] and covalent organic frameworks (COFs)[35-41] have been used to recover precious metals such as Au(III), Pt(IV), and Pd(II) from aqueous solution. On the basis of host–guest interactions, various strategies have been developed to improve metal-binding affinity and afford high adsorption capacity and selectivity. For palladium ions, the common approaches include building noncovalent interactions and cooperative interactions. In general, Pd(II) adopts a square-planar coordination geometry, involving four N, four O, or two O and two N atoms of organic ligands to produce a planar [Pd(II)N_4], [Pd(II)O_4], or [Pd(II)N_2O_2] units, respectively (Figure 1a).[42,43] In a recent notable contribution, this palladium chelation strategy was adopted in the development of COF materials for the extraction of Pd(II) under mild conditions.[41] However, despite tremendous efforts to maximize the binding affinity between palladium ions and adsorbents, few adsorbents are capable of selectively capturing Pd(II) under highly acidic and high ionic strength conditions.

Herein, to accomplish this ambitious task, we proposed and validated the design of COFs containing single-ion traps for the recognition and efficient recovery of Pd(II) from acidic waste solutions and laboratory waste. First, we observed that the traditional eclipsed (AA) stacking configuration of a parent COF created Pd(II) cheating sites with only two electron-donating atoms (N, or O) from organic linkers (Figure 1b), and two further O atoms from NO_3^- ions or solvent molecules completing a square-planar coordination. However, the electron-donating contribution from interlayer atoms was limited and could not be utilized effectively due to the overlap of the parallel sites. With these considerations in mind, we envisaged that by converging cooperative functions into the nanospace of COFs, it should be possible to boost the host–guest interactions; thus, enhancing the recognition and dynamic uptake efficiency of Pd(II) under extreme conditions. Therefore, a robust COF (denoted as ACOF-1) with an antiparallel stacked structure was designed and synthesized in this contribution (Figures 1b,c). Benefiting from its large porosity, hydrophilicity, specific Pd(II) binding affinity, and interlayer synergetic (Lewis base sites serving as single-ion traps, Figure 1d), ACOF-1 exhibited the highest Pd(II) uptake (412.9 ± 14.2 mg/g) among top-performing adsorbents in 3M HNO_3. Subsequent breakthrough experiments revealed that ACOF-1 could efficiently recover Pd(II) from laboratory waste liquid. The calculated dynamic adsorption capacities reached as high as 232.9 and 320.9 mg/g in 3M HNO_3 and laboratory waste, respectively. Moreover, ACOF-1 was regenerated readily and recycled with negligible losses in palladium recovery, maintaining its structure after elution. These results demonstrated the feasibility of the single-ion trap strategy for the selective capture of Pd(II) under extreme conditions, guiding the future rational design of novel adsorbents for the recovery of other precious metals.

Experimental Methods

Synthesis of ACOF-1

In a typical synthesis, 2,5-bis(3-hydroxypropoxy) terephthalohydrazide (BHTH, 34.2 mg) and 5,5′,5″-(benzene-1,3,5-triyl)tripicolinaldehyde (BTPA, 39.3 mg) were

DOI: 10.31635/ccschem.023.202303404
Citation: *CCS Chem.* **2024**, 6, 1908–1919
Link to VoR: https://doi.org/10.31635/ccschem.023.202303404

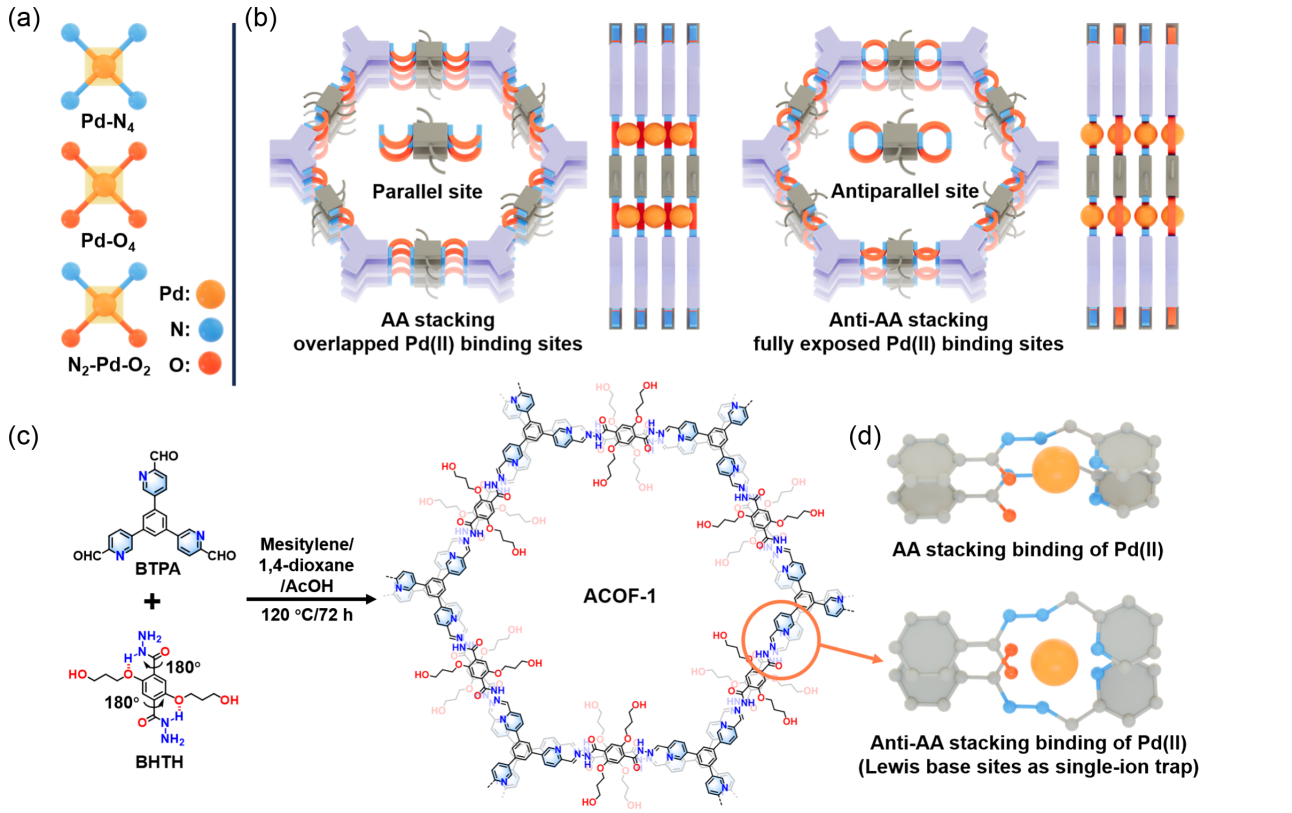

Figure 1 | *(a) Schematic illustration of planar [Pd(II)N_4], [Pd(II)O_4], or [Pd(II)N_2O_2] units. (b) Schematic illustration of traditional AA stacking (left) and antiparallel AA (anti-AA) stacking (right) in COF adsorbents, showing how antiparallel stacked layers form fully exposed Pd(II) binding sites, significantly enhancing the utilization and affinity of binding sites. (c) Illustration of the synthesis of ACOF-1 with Lewis base sites as single-ion traps. (d) Illustration showing Pd(II) binding in the AA and anti-AA stacked structures. COF, covalent organic framework; ACOF-1, antiparallel stacked covalent organic framework.*

dissolved in a mixture of 1,4-dioxane (1 mL)/mesitylene (1 mL)/acetic acid (AcOH, 6 M, 0.2 mL) in a 5 mL glass ampoule tube, then transferred to an ultrasonic device. After 30 min of ultrasound, the ampoule tube was frozen and sealed in a N_2 atmosphere, followed by heating in an oven at 120 °C for 3 days, which yielded pale yellow powder (ACOF-1) after filtration, washing with ethanol and acetone, and finally, drying at 35 °C.

Synthesis of ACOF-2

In a typical synthesis, BHTH (17.1 mg) and 5′-(4-formylphenyl)-[1,1′:3′,1″-terphenyl]-4,4″-dicarbaldehyde (TFPB, 19.5 mg) were dissolved in a mixture of 1,4-dioxane (0.5 mL)/mesitylene (0.5 mL)/AcOH (6 M, 0.1 mL) in a 5 mL glass ampoule tube, then transferred to an ultrasonic device. After 30 min of ultrasound, the ampoule tube was frozen and sealed in a N_2 atmosphere, followed by heating in an oven at 120 °C for 3 days, which yielded pale yellow powder (ACOF-2) after filtration, washing with ethanol and acetone, and finally, drying at 35 °C.

Results and Discussion

Synthesis of antiparallel stacked COF

As shown in Figure 1c, antiparallel stacked ACOF-1 was synthesized through condensation of BTPA and BHTH under the solvothermal condition in mesitylene/1,4-dioxane (1/1, by volume) using AcOH as the catalyst at 120 °C for 3 days. The chemical structure of the as-synthesized ACOF-1 was determined by Fourier-transformed infrared (FT-IR) spectroscopy and ^{13}C solid-state cross-polarization magic angle spinning nuclear magnetic resonance (^{13}C CP/MAS NMR) spectroscopy. The appearance of an FT-IR peak at 1667 cm^{-1}, attributed to an imine C=N stretching mode, together with the disappearance of –CHO signal at 1702 cm^{-1} characteristic of BTPA, suggested the complete reaction of the starting reagents (Figure 2a).[44,45] The ^{13}C CP/MAS NMR spectrum of ACOF-1 showed an imine C=N peak at 152 ppm (Figure 2b), further confirming the aldimine condensation reaction between BTPA and BHTH. The ^{13}C NMR

DOI: 10.31635/ccschem.023.202303404
Citation: *CCS Chem.* **2024**, 6, 1908–1919
Link to VoR: https://doi.org/10.31635/ccschem.023.202303404

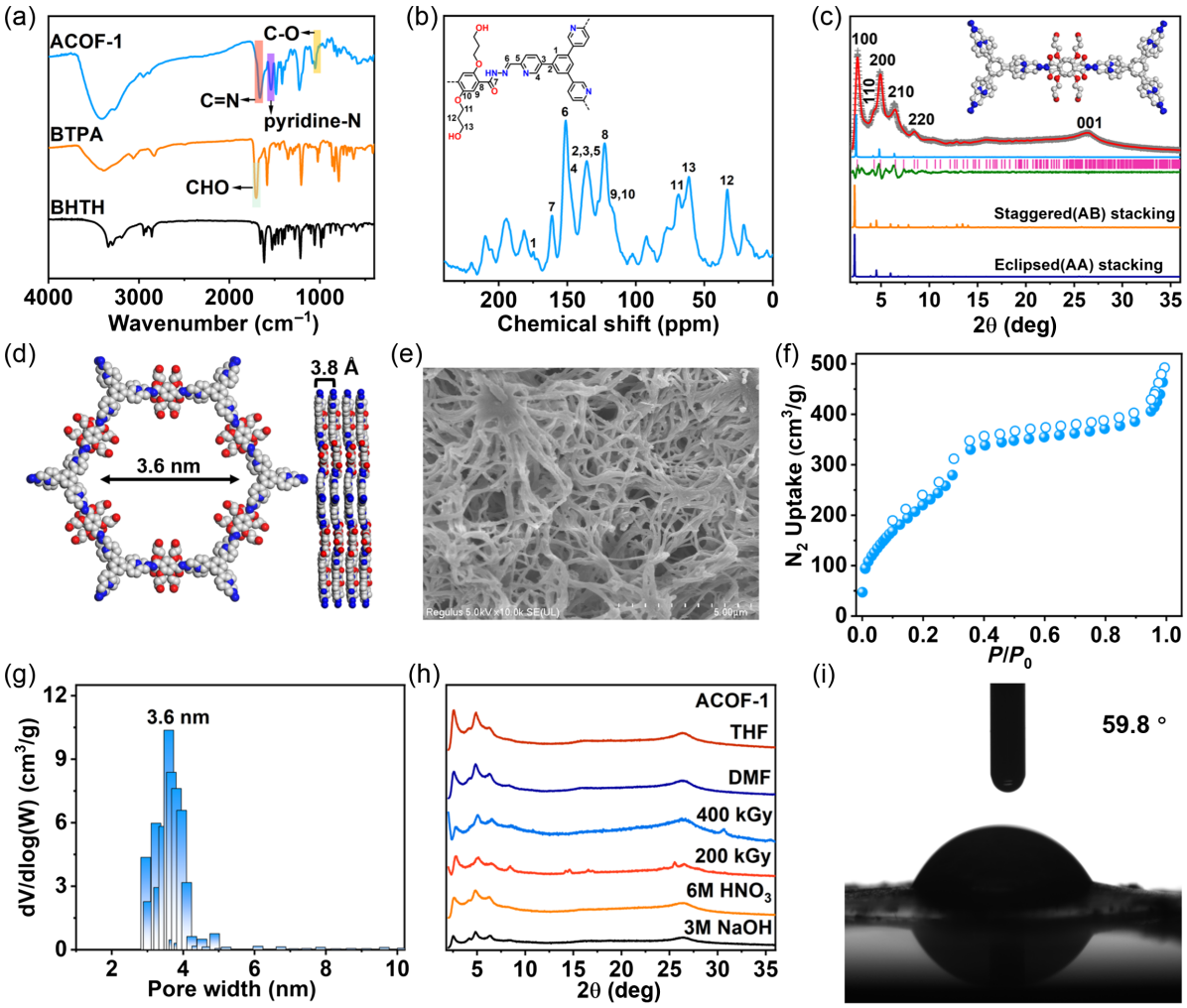

Figure 2 | *(a) FT-IR spectra of ACOF-1 and used linkers. (b) ^{13}C CP/MAS solid-state NMR spectra of ACOF-1. (c) Experimental PXRD pattern of ACOF-1 with corresponding Pawley refinement (red), antiparallel AA stacking simulated results (blue), and Bragg positions (pink) showing good fits to the experimental data (gray) with minimal differences (green). The inset shows the structural model of ACOF-1 assuming the antiparallel AA stacking configuration. Simulation results based on eclipsed AA (navy) and staggered AB (orange) stacking configurations were used for comparison. (d) Top and side view of the antiparallel AA stacking crystal structures of ACOF-1. (e) SEM image of ACOF-1. (f,g) N_2 sorption isotherms and pore size distributions measured at 77 K for ACOF-1. (h) PXRD patterns of ACOF-1 after treatment under different conditions for 24 h. (i) Contact angle for the water droplet on a pressed pellet of ACOF-1. FT-IR, Fourier-transformed infrared; ACOF-1, antiparallel stacked covalent organic framework; ^{13}C CP/MAS solid-state NMR, magic angle spinning solid-state carbon-13 nuclear magnetic resonance; SEM, scanning electron microscopy; PXRD, powder X-ray diffraction.*

signals at 69, 61, and 33 ppm, associated with the carbon-hydroxyl chain, further verified the formation of polymeric frameworks.[46]

Next, powder X-ray diffraction (PXRD) and Pawley refinement analyses were conducted to study the crystallinity of ACOF-1. The PXRD pattern of ACOF-1 exhibited intense peaks at 2θ = 2.49°, 4.21°, 4.92°, 6.40°, 8.43°, and 26.37° (Figure 2c), which could readily be assigned to diffraction on (100), (110), (200), (210), (220), and (001) planes, respectively. Pawley refinement revealed ACOF-1 to crystallize in the P6cc space group with lattice parameters of $a = b = 42.3108$ Å, $c = 7.2582$ Å, $\alpha = \beta = 90°$, and $\gamma = 120°$, together with the negligible profile differences ($R_{wp} = 4.49\%$, $R_p = 3.16\%$) (Supporting Information Table S1). The structural simulation matches the antiparallel AA stacking structural models well (Figures 2c,d and Supporting Information Figure S1). The theoretical layer distance and pore diameter in ACOF-1 are ~3.8 Å and ~3.6 nm, respectively. To further probe the stacking structure, we built other possible models by arranging linkers in eclipsed AA stacking and staggered AB stacking configurations (Figure 2c and Supporting

DOI: 10.31635/ccschem.023.202303404
Citation: *CCS Chem.* **2024**, 6, 1908–1919
Link to VoR: https://doi.org/10.31635/ccschem.023.202303404

Information Figure S1). In contrast, the simulated PXRD pattern for the eclipsed AA stacking exhibited intense peaks at 2θ = 2.26°, 3.92°, 4.53°, 5.99°, 6.79°, 7.87°, and 25.04° corresponding to (100), (110), (200), (120), (210), (220), and (001) planes, respectively, and showed additional differences to the experimental pattern on ACOF-1 in the 2θ range between 10° and 20°. Further, the staggered AB stacking could be ruled out by comparing the experimental and simulated PXRD patterns from 2θ ~10° to 15°, whereas the simulated PXRD pattern of the antiparallel structure was in excellent accord with the experimental PXRD pattern. Taken together, the simulated PXRD patterns for the eclipsed AA stacking and staggered AB stacking configurations were inconsistent with the experimental PXRD signal for ACOF-1. The fact that ACOF-1 crystallized in the antiparallel AA stacking mode was likely due to intramolecular hydrogen bonding involving the BHTH linker (N–H···O), which plays a decisive role in the orientation of the hydrazine groups on the linkers (Figure 1c).[47-49] Moreover, the repulsion between oxygen atoms of carbonyl groups in adjacent layers was expected to assist crystallization in a reverse parallel stacking configuration.[49,50] Scanning electron microscopy (SEM) revealed ACOF-1 to possess a nanowire morphology (Figure 2e).

Porosity and stability properties

The porosity of ACOF-1 was determined from nitrogen sorption isotherms collected at 77 K for activated samples. As shown in Figure 2f, ACOF-1 demonstrated a typical type-II isotherm with a steep uptake at P/P_0 from 0.05 to 0.35, suggesting mesoporous character. The calculated Brunauer–Emmett–Teller (BET) surface area was approximately 900 m^2/g. The pore size was estimated to be ~3.6 nm using a nonlocal density functional theory (NLDFT) method, which perfectly matched its theoretical value of 3.6 nm (Figure 2g). Thermogravimetric analysis (TGA) revealed that ACOF-1 possesses good thermal stability up to 300 °C under a N_2 atmosphere (Supporting Information Figure S2). The chemical stability of ACOF-1 was investigated by immerging samples in tetrahydrofuran (THF), dimethylformamide (DMF), 3M NaOH, and 6M HNO_3, respectively. The PXRD patterns showed the crystalline structure of the framework was largely retained (intensities slightly reduced) after all these treatments (Figure 2h). The extraction of palladium from spent nuclear fuel (high radioactivity) is a promising alternative method for obtaining large amounts of palladium. Therefore, we next studied the radiation resistance of ACOF-1 by exposing the sample to γ-rays. PXRD confirmed that the integrity of the framework was retained (intensities slightly reduced) after 200 and 400 kGy γ-ray doses (Figure 2h). The surface wettability of ACOF-1 was probed by water contact angle measurements. The contact angle of a water droplet on ACOF-1 was 59.8°, suggesting hydrophilic properties (Figure 2i). Taken together, the specific structural features, large porosity, and excellent stability of ACOF-1 suggest the potential for use as an adsorbent for metal extraction, such as Pd(II) recovery for waste aqueous solutions. Therefore, we next conducted a series of experiments to assess the adsorption performance of ACOF-1 toward Pd(II) under various conditions.

To validate the utility of the single-ion traps in ACOF-1 for Pd(II) recovery, we synthesized an isostructural ACOF-2 by reaction of TFPB and BHTH at 120 °C. The synthesis and characterization data for ACOF-2 are provided in the Supporting Information (Supporting Information Figures S3–S12 and Table S2). ACOF-2 showed a similar structure to ACOF-1 but did not contain any pyridine N units in the framework.

Pd(II) adsorption studies

To evaluate the Pd(II) recovery ability of the COFs, preliminary experiments were carried out in 3M HNO_3 solutions to determine the optimal adsorbent/liquid ratio, adsorption capacity, and adsorption kinetics. An adsorbent/liquid ratio of 0.5 g/L was used for subsequent adsorption experiments (Figure 3a). Next, the Pd(II) adsorption ability of ACOF-1 was determined at initial HNO_3 concentrations ranging from 0.5 to 3M. ACOF-2, commercial D152, D101, Al_2O_3, and activated carbon were employed for comparison (Figure 3b). ACOF-1 showed a higher Pd(II) removal efficiency compared to ACOF-2 and the commercial adsorbents, suggesting excellent adsorption properties under super acidic environments (Figure 3b). To evaluate the adsorption capacity of the different adsorbents in 3M HNO_3, adsorption data were executed by varying the Pd(II) concentration from ~25 to 500 ppm. After 24 h, the adsorption capacity of ACOF-1 was 412.9 ± 14.2 mg/g, which exceeded its structural analogue ACOF-2 (220.2 ± 14.2 mg/g) under the same conditions (Figure 3c). The adsorption isotherm curves fitted well with the Langmuir model, indicating a monolayer adsorption process (Figure 3c and Supporting Information Table S3). As shown in Figure 3d, most reported studies have focused on the extraction of Pd(II) in relatively weak acid solutions, with only a few studies examining Pd(II) recovery in such highly acidic media. Nevertheless, the adsorption capacity of ACOF-1 exceeded other previously reported sorbents in 3M HNO_3 (Figure 3d and Supporting Information Table S4).[11,21-25,27,29,31-34,39,41,51-55] Next, kinetic isotherms were obtained in ~100 ppm Pd(II)/3M HNO_3 solutions, with ACOF-1 demonstrating extremely rapid kinetics, achieving a palladium uptake of 176.4 ± 6.2 mg/g within 100 min (Figure 3e). Furthermore, the adsorption data followed a pseudo-second-order kinetic model exhibiting a perfect linear relationship with a high correlation coefficient R^2 (>0.99), suggesting that the Pd(II)

DOI: 10.31635/ccschem.023.202303404
Citation: *CCS Chem.* **2024**, 6, 1908–1919
Link to VoR: https://doi.org/10.31635/ccschem.023.202303404

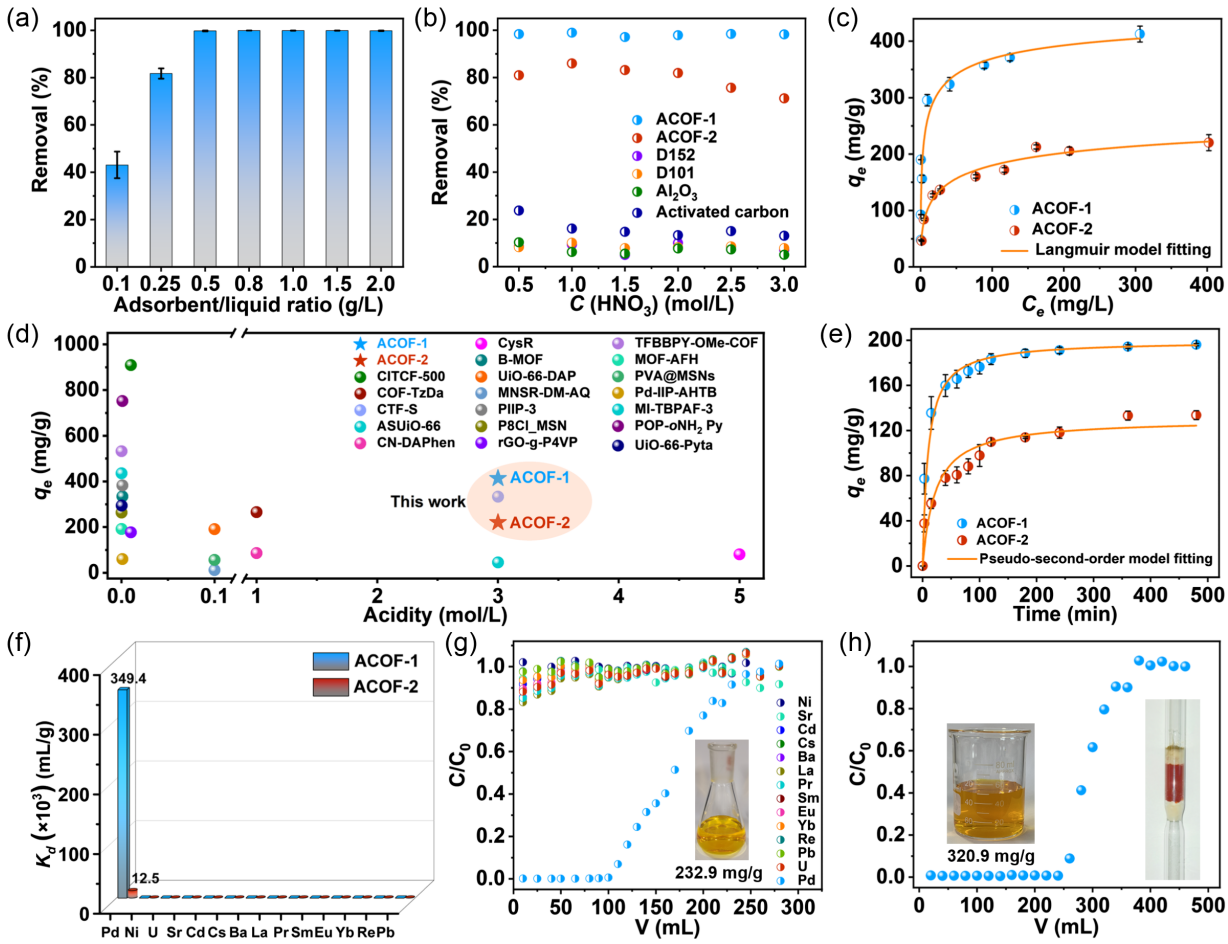

Figure 3 | *(a) Pd(II) removal by ACOF-1 at various adsorbent/liquid ratios. (b) Effect of initial HNO_3 concentration on the removal of Pd(II) by ACOF-1, ACOF-2, and commercial adsorbents (D152, D101, Al_2O_3, and activated carbon). (c) Sorption isotherms of Pd(II) by ACOF-1 and ACOF-2. (d) The comparison of saturated Pd(II) uptake capacities for various adsorbents. (e) Pd(II) adsorption kinetics on ACOF-1 and ACOF-2 at an initial Pd(II) concentration of ~100 ppm. (f) Selectivity of ACOF-1 and ACOF-2 for different cations in simulated HLLW solution. (g) Experimental column breakthrough curves for simulated high-level liquid waste solution (acidity ~3M HNO_3) by ACOF-1 (the inset shows the palladium eluted from the used column after successive washings with a mixture of thiourea/HCl). (h) Breakthrough curves for a laboratory waste liquid by ACOF-1 (the inset shows the palladium adsorbed to the column and then eluted from the column after adsorption). ACOF-1/2, antiparallel stacked covalent organic frameworks; HLLW, high-level liquid nuclear waste;*

adsorption by ACOF-1 involves chemical adsorption (Figure 3e and Supporting Information Table S5). ACOF-2 showed relatively slow kinetics and much lower adsorption capacities under similar conditions, which confirmed the key role of single-ion traps formed by the antiparallel AA stacking in ACOF-1.

The excellent adsorption performance of ACOF-1 encouraged us to assess the Pd(II) adsorption selectively in the presence of other competing metal ions, such as Cs (I), Ba(II), Cd(II), Ni(II), Sr(II), La(III), Pr(III), Pb(II), U(VI), and so on. Therefore, we carried out the Pd(II) adsorption experiments in a simulated high-level liquid waste solution (acidity ~3M HNO_3) (Supporting Information Table S6). The calculated distribution coefficient (K_d) and removal efficiency of ACOF-1 toward Pd(II) were ~349.4×10^3 mL/g and >99.4%, respectively, much higher than the values determined for the other metal ions, suggesting a specific binding affinity for Pd(II) (Figure 3f and Supporting Information Figure S13). Significantly, the Pd(II) adsorbed ACOF-1 could be easily eluted by using a mixture of 0.5 mol/L thiourea/0.5 mol/L HCl solutions, and over 94% Pd(II) removal retained after the recycle test (Supporting Information Figure S14). The Pd(II) removal efficiency of ACOF-1 was unaffected by 200 and 400 kGy γ-radiation doses, confirming its excellent radiation stability (Supporting Information Figure S15). PXRD and FT-IR showed that ACOF-1 retained its crystallinity after Pd(II)

DOI: 10.31635/ccschem.023.202303404
Citation: *CCS Chem.* **2024**, 6, 1908–1919
Link to VoR: https://doi.org/10.31635/ccschem.023.202303404

adsorption experiments and elution (Supporting Information Figure S16).

Next, dynamic Pd(II) breakthrough experiments were conducted using a simulated HLLW acidic solution to simulate the treatment of acidic waste containing Pd(II). As a result, ACOF-1 can effectively adsorption of Pd(II) from 3M HNO_3, reaching equilibrium after treatment with 280 mL of solution (Figure 3g), with a dynamic uptake capacity as high as 232.9 mg/g (Figure 3g). Other metal ions quickly eluted through the ACOF-1 packed column, again confirming the preferential uptake of Pd(II).

Chemical reactions and catalysis experiments can produce a lot of palladium-containing waste liquids in a chemistry laboratory. By recycling such lab waste, the need to mine new palladium can be reduced. Therefore, we next carried out Pd(II) adsorption experiments in organic solvents containing dissolved Pd(II) and also Pd-containing laboratory wastes (including H_2O, ethanol, ethyl acetate, Na^+, Ni^{2+}, UO_2^{2+}, NO_3^-, etc.). The adsorption efficiencies of ACOF-1 for Pd(II) in ethyl acetate and ethanol were ~99.5% and 99.2%, respectively (Supporting Information Figure S17). Commercial adsorbent materials showed much lower removal efficiencies under similar conditions. Then we evaluated Pd(II) adsorption performance by ACOF-1 in laboratory waste. The breakthrough volume for Pd(II) was 380 mL, with the adsorption capacity being 320.9 mg/g (Figure 3h). The excellent selectivity and high capacity suggest that ACOF-1 was a promising adsorbent for Pd(II) recovery from palladium-containing organic solutions and lab wastes.

Adsorption mechanism

After showing the excellent Pd(II) recovery performance of the ACOF-1 in 3M HNO_3 and laboratory waste streams, we next attempted to gain an in-depth understanding of the Pd(II) adsorption mechanism by carrying out X-ray photoelectron spectroscopy (XPS), X-ray absorption spectroscopy (XAS), DFT calculations, and molecular dynamics (MD) simulations. XPS spectra revealed the presence of intense Pd signals after the adsorption experiments (Supporting Information Figure S18). Compared with the N 1s spectrum of ACOF-1 (which showed three distinct nitrogen environments as expected based on the COF's structure), a new N 1s signal appeared around 406.5 eV after Pd(II) adsorption, which could readily be assigned to charge-balancing NO_3^- ions, suggesting the coordination of Pd(II) involved NO_3^- (Figure 4a). The Pd 3d spectrum of ACOF-1, following palladium adsorption showed peaks at 338.6 and 343.8 eV in a 3:2 area ratio, assigned to the Pd $3d_{5/2}$ and Pd $3d_{3/2}$ signals of Pd(II) (Figure 4b).[56] No Pd(0) was detected, indicating that Pd(II) was not reduced by the COF during adsorption. The Pd K-edge X-ray absorption near-edge structure (XANES) spectrum of ACOF-1 after Pd(II) adsorption was similar to those collected for the PdO and $PdCl_2$ reference samples, with the edge position being typical for Pd(II), consistent with the XPS results (Figure 4c). The Fourier-transformed extended X-ray absorption fine structure (EXAFS) spectrum exhibited a main peak at ~1.6 Å in R space, which was assigned to Pd-N/Pd-O bonds formed between the single-ion traps and Pd(II) (Figure 4d).[25] Fitting the curve indicated a local Pd(II) environment including one NO_3^- ion, one oxygen atom, and two nitrogen atoms from the single-ion traps (Figure 4e–g and Supporting Information Table S7). Furthermore, the EXAFS wavelet transform analyses exhibited a maximum intensity of 7.0 $Å^{-1}$ in k space (together with 1.6 Å in R space), consistent with Pd-N and Pd-O contributions and providing further evidence for a square-planar [Pd(II) N_2O_2] coordination (Figure 4h).

Next, Gibbs free energy changes (ΔG) associated with the binding of Pd(II) to the various possible adsorption sites in ACOF-1 were calculated and compared to better understand the adsorption mechanism. Figure 5a shows the thermodynamically feasible coordination geometries and corresponding Gibbs free energy changes. Pd(II) binding to the single-ion traps in ACOF-1 offered the lowest ΔG value of −34.37 kcal/mol, much lower than other hypothetical coordination modes, revealing that the extra layer of antiparallel AA stacking generated hydrogen bonding with the single Pd(II) ion trap, stabilizing the system. These results suggested the single-ion traps identified by EXAFS offered the strongest binding affinity towards Pd(II). Subsequently, we explored the adsorption dynamics of Pd^{2+} on ACOF-1 in HNO_3 solutions by using MD simulations. Ni^{2+} and UO_2^{2+} ions were selected as the competing ions for the simulation. The molar ratio of Pd^{2+}: Ni^{2+}: UO_2^{2+} used in the simulation was 1.5:1:1. The simulation revealed that Pd^{2+} was adsorbed into the channels of ACOF-1 after immersing the sample in solution within 20 ns, while Ni^{2+} and UO_2^{2+} passed through the sample without adsorption (Figure 5b). After ~60 ns, the adsorbed amount of Pd^{2+} increased with almost no other adsorbed cations, indicating an extraordinary affinity for Pd^{2+} even at high concentrations of other competing ions. At ~100 ns, the amount of adsorbed Pd^{2+} greatly exceeded adsorbed Ni^{2+} and UO_2^{2+}, verifying a high binding affinity toward Pd^{2+} in the HNO_3 solution. Moreover, Figure 5c–e shows the nonbonded interaction energy diagrams for Pd^{2+}/ACOF-1, UO_2^{2+}/ACOF-1, and Ni^{2+}/ACOF-1 during the MD simulation. The calculated Van der Waals interaction between Pd^{2+} and the COF was −1.89 kJ/mol, whilst the Coulombic interaction between Pd^{2+} and ACOF-1 was −16.20 kJ/mol (Figure 5c). Combining the two contributions, the total intermolecular interaction energy between Pd^{2+} and the COF was −18.10 kJ/mol, higher than that of Ni^{2+}/ACOF-1 (−3.31 kJ/mol) and UO_2^{2+}/ACOF-1 (−14.18 kJ/mol). The

DOI: 10.31635/ccschem.023.202303404
Citation: *CCS Chem.* **2024**, 6, 1908–1919
Link to VoR: https://doi.org/10.31635/ccschem.023.202303404

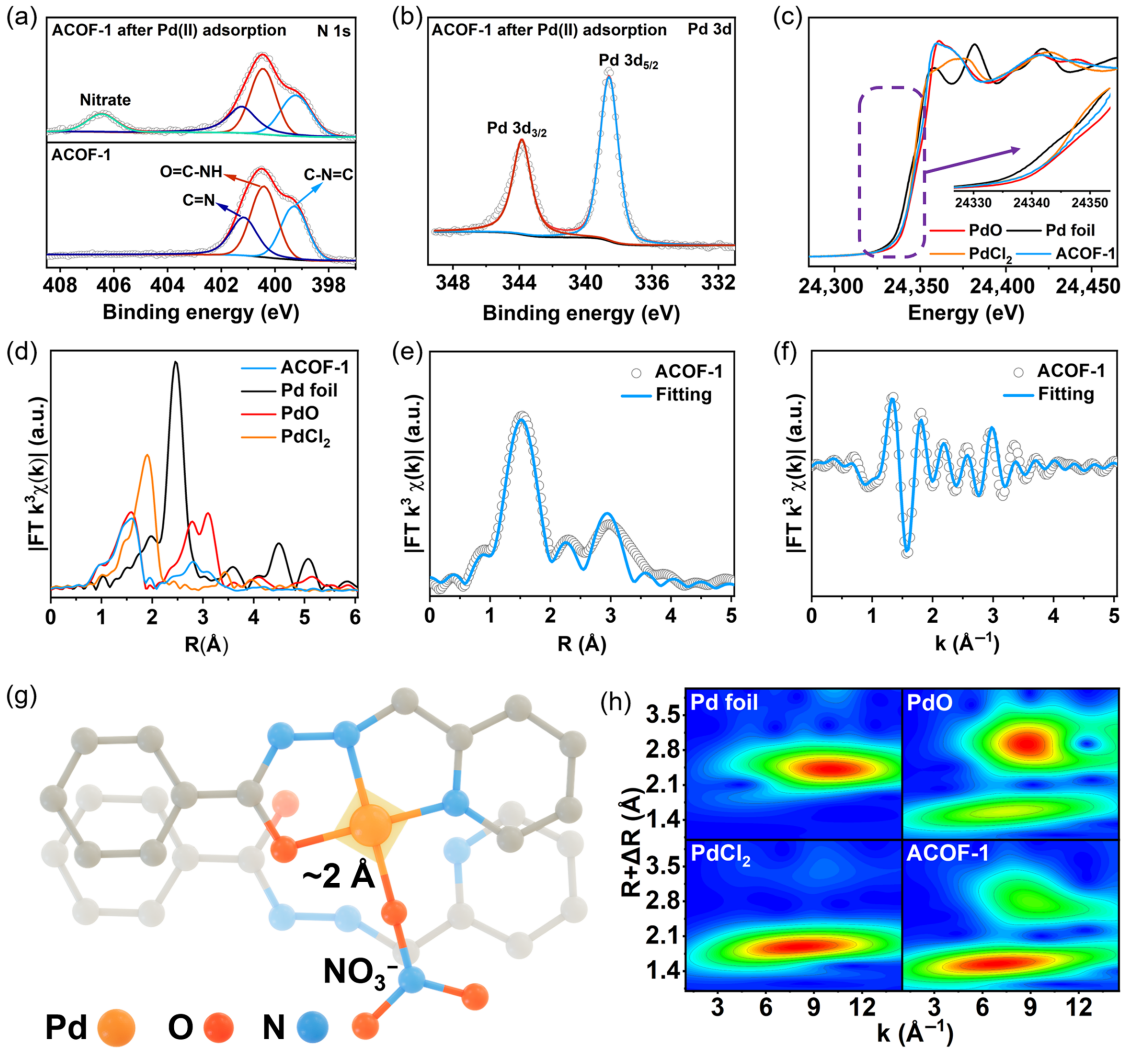

Figure 4 | *(a) N 1s XPS spectra of ACOF-1 before and after adsorption of Pd(II). (b) Pd 3d XPS spectrum of ACOF-1 after adsorption of Pd(II). (c) Pd K-edge XANES spectra for ACOF-1 after adsorption of Pd(II) and references. (d) Pd K^2-weighted χ(k) function of EXAFS spectra for ACOF-1 after adsorption of Pd(II) and references. (e, f) Fitting curves for ACOF-1 after adsorption of Pd(II). (g) The ACOF-1 structure used as a model for the EXAFS analysis. The Pd atom (orange sphere) is bound with two N atoms (blue spheres), one O atom (red sphere) from ACOF-1, and one oxygen atom from NO_3^- to form a square-planar [Pd(II)N_2O_2] unit. (h) Wavelet transform contour plots for ACOF-1 after adsorption of Pd(II). Pd foil, PdO, and $PdCl_2$ were employed as reference materials in panels c–h. XPS, X-ray photoelectron spectroscopy; ACOF-1, antiparallel stacked covalent organic framework; EXAFS, extended X-ray absorption fine structure.*

results further verified the strong binding affinity between Pd(II) ions and single ion traps of ACOF-1 (Figure 5c–e). The sorption data, spectroscopic data, and theoretical calculation results revealed the excellent adsorption performance of ACOF-1 toward Pd(II) ions under super acidic and high ionic strength conditions.

The aforementioned results validated our "single-ion trap" strategy that involved building electron-donating (Lewis base) sites into the COF for palladium recovery under extreme conditions. This approach took advantage of the antiparallel stacking manner of the ACOF-1 framework, which effectively utilized the cooperation between the hydrazine-carbonyl sites and pyridine sites (creating single-ion traps for Pd(II) ions). The single-ion trapped coordinate Pd(II) in a square-planar mode, forming the stable [Pd(II)N_2O_2] units; thus, ensuring a strong binding affinity for Pd(II). The developed ACOF-1 overcame the long-term challenge of Pd(II) recovery under super acidic and high ionic strength conditions. High dynamic adsorption capacities and efficiency were obtained in column experiments under practical conditions. These results demonstrated how slight modifications to COF adsorbents could greatly enhance their performance for selective metal ion capture. The results suggested that

DOI: 10.31635/ccschem.023.202303404
Citation: *CCS Chem.* **2024**, 6, 1908–1919
Link to VoR: https://doi.org/10.31635/ccschem.023.202303404

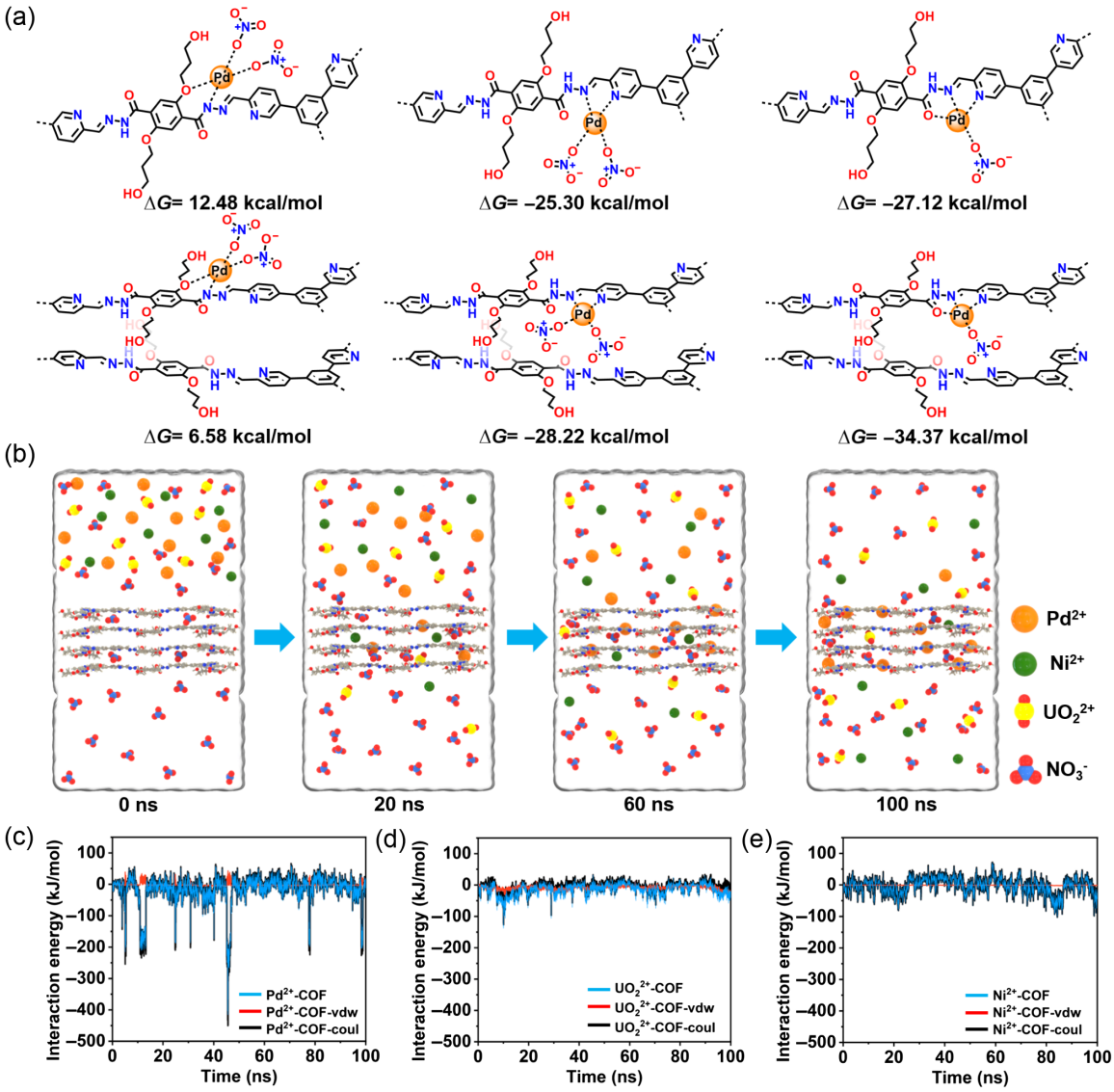

Figure 5 | *(a) Models for Pd^{2+} binding to different sites in ACOF-1 and the corresponding Gibbs free energy changes (ΔG). (b) Selected snapshots from the MD simulation showing the Pd^{2+} adsorption process on ACOF-1 in HNO_3 solution. (c) Time evolution of the nonbonded interaction energies between COF and Pd^{2+} (Pd^{2+}-COF, total energy of intermolecular interaction; Pd^{2+}-COF-vdw, Van der Waals interaction between Pd^{2+} and COF; Coulomb interaction between Pd^{2+} and COF). (d) Time evolution of the nonbonded interaction energies between COF and UO_2^{2+} (UO_2^{2+}-COF, total energy of intermolecular interaction; UO_2^{2+}-COF-vdw, Van der Waals interaction between UO_2^{2+} and COF; Coulomb interaction between UO_2^{2+} and COF). (e) Time evolution of the nonbonded interaction energies between COF and Ni^{2+} (Ni^{2+}-COF, total energy of intermolecular interaction; Ni^{2+}-COF-vdw, Van der Waals interaction between Ni^{2+} and COF; Coulomb interaction between Ni^{2+} and COF). ACOF-1, antiparallel stacked covalent organic framework; MD, molecular dynamics.*

ACOF-1 is a promising adsorbent for industrial palladium recovery applications.

Conclusion

We have successfully developed an antiparallel stacked COF-based adsorbent containing single-ion traps for Pd(II) recovery from aqueous solutions. The single-ion traps formed from interlayer atoms showed cooperative electron-donating contributions, which exhibited a significant effect on selective Pd(II) adsorption and separation performance. The developed ACOF-1 demonstrated good stability, high adsorption capacity, selectivity, and reusability toward Pd(II) under extreme conditions. To the best of our knowledge, this work represents the first report of a COF capable of Pd(II) recovery in 3M HNO_3

DOI: 10.31635/ccschem.023.202303404
Citation: *CCS Chem.* **2024**, 6, 1908–1919
Link to VoR: https://doi.org/10.31635/ccschem.023.202303404

and organic waste liquids containing palladium residues. We expect that this work will provide a new design concept for solid adsorbents for palladium (and other precious metals) recovery from waste.

Supporting Information

Supporting Information is available and includes additional chemicals, instrumentation, crystallographic data, FT-IR spectra, solid-state ^{13}C CP/MAS NMR spectra, PXRD patterns, TGA curves, N_2 sorption and pore size analysis, SEM images, contact angle, XPS spectra, Pd(II) extraction experimental details, adsorption data and fitting results, XAS fitting results, DFT calculations, and MD simulation.

Conflict of Interest

There is no conflict of interest to report.

Acknowledgments

This work was supported by the National Natural Science Foundation of China (NSFC; grant nos. U2167218, 22322603, and 22276054), the Beijing Outstanding Young Scientist Program, the Robert A. Welch Foundation (grant no. B-0027), and the New Zealand James Cook Research Fellowship. We thank Shiyanjia Lab (https://www.shiyanjia.com) for expert assistance with the DFT calculations and MD simulations.

References

1. Gao, C.; Lyu, F.; Yin, Y. Encapsulated Metal Nanoparticles for Catalysis. *Chem. Rev.* **2021**, *121*, 834–881.
2. Wang, L.; Zeng, Z. H.; Gao, W. P.; Maxson, T.; Raciti, D.; Giroux, M.; Pan, X. Q.; Wang, C.; Greeley, J. Tunable Intrinsic Strain in Two-Dimensional Transition Metal Electrocatalysts. *Science* **2019**, *363*, 870–874.
3. Sehnal, P.; Taylor, R. J. K.; Fairlamb, I. J. S. Emergence of Palladium(IV) Chemistry in Synthesis and Catalysis. *Chem. Rev.* **2010**, *110*, 824–889.
4. Yu, P.; Zeng, Q. S.; Zhu, C.; Zhou, L. J.; Zhao, W. N.; Tong, J. C.; Liu, Z.; Yang, G. W. Ternary Ta_2PdS_6 Atomic Layers for an Ultrahigh Broadband Photoresponsive Phototransistor. *Adv. Mater.* **2021**, *33*, 2005607.
5. Guo, H.; Yang, C. Y.; Zhang, X. H.; Motta, A.; Feng, K.; Xia, Y.; Shi, Y. Q.; Wu, Z.; Yang, K.; Chen, J. H.; Liao, Q. G.; Tang, Y. M.; Sun, H. L.; Woo, H. Y.; Fabiano, S.; Facchetti, A.; Guo, X. G. Transition Metal-Catalysed Molecular N-Doping of Organic Semiconductors. *Nature* **2021**, *599*, 67–73.
6. Li, Y. S.; Loh, L.; Li, S. F.; Chen, L.; Li, B. C.; Bosman, M.; Ang, K. W. Anomalous Resistive Switching in Memristors Based on Two-Dimensional Palladium Diselenide Using Heterophase Grain Boundaries. *Nat. Electron.* **2021**, *4*, 348–356.
7. Tang, J. L.; Zuo, Y.; Tang, Y. M.; Xiong, J. P. The Preparation of Corrosion Resistant Palladium Films on 316L Stainless Steel by Brush Plating. *Surf. Coat. Technol.* **2010**, *204*, 1637–1645.
8. Medici, S.; Peana, M.; Nurchi, V. M.; Lachowicz, J. I.; Crisponi, G.; Zoroddu, M. A. Noble Metals in Medicine: Latest Advances. *Coord. Chem. Rev.* **2015**, *284*, 329–350.
9. Sepehrpour, H.; Fu, W. X.; Sun, Y.; Stang, P. J. Biomedically Relevant Self-Assembled Metallacycles and Metallacages. *J. Am. Chem. Soc.* **2019**, *141*, 14005–14020.
10. KITCO. https://www.kitco.comchartslivepalladium.html (February 2022).
11. Song, K. S.; Ashirov, T.; Talapaneni, S. N.; Clark, A. H.; Yakimov, A. V.; Nachtegaal, M.; Coperet, C.; Coskun, A. Porous Polyisothiocyanurates for Selective Palladium Recovery and Heterogeneous Catalysis. *Chem* **2022**, *8*, 2043–2059.
12. Zhang, L.; Song, Q.; Liu, Y.; Xu, Z. An Integrated Capture of Copper Scrap and Electrodeposition Process to Enrich and Prepare Pure Palladium for Recycling of Spent Catalyst from Automobile. *Waste Manag.* **2020**, *108*, 172–182.
13. Zhang, Y.; He, L.; Pan, T.; Xie, J.; Wu, F.; Dong, X.; Wang, X.; Chen, L.; Gong, S.; Liu, W.; Kang, L.; Chen, J.; Chen, L.; Chen, L.; Han, Y.; Wang, S. Superior Iodine Uptake Capacity Enabled by an Open Metal-Sulfide Framework Composed of Three Types of Active Sites. *CCS Chem.* **2022**, *5*, 1540–1548.
14. Ruhela, R.; Singh, A. K.; Tomar, B. S.; Hubli, R. C. Separation of Palladium from High Level Liquid Waste—A Review. *RSC Adv.* **2014**, *4*, 24344–24350.
15. Chen, Y.; Xu, M. J.; Wen, J. Y.; Wan, Y.; Zhao, Q. F.; Cao, X.; Ding, Y.; Wang, Z. L.; Li, H. X.; Bian, Z. F. Selective Recovery of Precious Metals Through Photocatalysis. *Nat. Sustain.* **2021**, *4*, 618–626.
16. Kim, M. S.; Kim, E. Y.; Jeong, J.; Lee, J. C.; Kim, W. Recovery of Platinum and Palladium from the Spent Petroleum Catalysts by Substrate Dissolution in Sulfuric Acid. *Mater. Trans.* **2010**, *51*, 1927–1933.
17. Dominguez-Benetton, X.; Varia, J. C.; Pozo, G.; Modin, O.; Ter Heijne, A.; Fransaer, J.; Rabaey, K. Metal Recovery by Microbial Electro-Metallurgy. *Prog. Mater. Sci.* **2018**, *94*, 435–461.
18. Maruyama, T.; Matsushita, H.; Shimada, Y.; Kamata, I.; Hanaki, M.; Sonokawa, S.; Kamiya, N.; Goto, M. Proteins and Protein-Rich Biomass as Environmentally Friendly Adsorbents Selective for Precious Metal Ions. *Environ. Sci. Technol.* **2007**, *41*, 1359–1364.
19. Chaudhuri, H.; Lin, X.; Yun, Y. S. Graphene Oxide-Based Dendritic Adsorbent for the Excellent Capturing of Platinum Group Elements. *J. Hazard. Mater.* **2023**, *451*, 131206.
20. Li, F.; Zhu, J.; Sun, P.; Zhang, M.; Li, Z.; Xu, D.; Gong, X.; Zou, X.; Geim, A. K.; Su, Y.; Cheng, H. M. Highly Efficient and Selective Extraction of Gold by Reduced Graphene Oxide. *Nat. Commun.* **2022**, *13*, 4472.
21. Gao, Y.; Zhou, R. Y.; Yao, L.; Wang, Y.; Yue, Q.; Yu, L.; Yu, J. X.; Yin, W. Selective Capture of Pd(II) from Aqueous Media by Ion-Imprinted Dendritic Mesoporous Silica Nanoparticles and Re-Utilization of the Spent Adsorbent for Suzuki Reaction in Water. *J. Hazard. Mater.* **2022**, *436*, 129249.

DOI: 10.31635/ccschem.023.202303404
Citation: *CCS Chem.* **2024**, 6, 1908–1919
Link to VoR: https://doi.org/10.31635/ccschem.023.202303404

22. Khusnun, N. F.; Hasan, N. S.; Amalina, I.; Jalil, A. A.; Firmansyah, M. L. Enhanced Recovery of Palladium from an Aqueous Solution Using an Ionic Liquid-Mesoporous Silica Composite in Batch and Fixed-Column Studies. *Ind. Eng. Chem. Res.* **2022**, *61*, 8634–8644.
23. Li, H.; Wu, F.; Pan, Y.; Zhang, Y.; Pleixats, R.; Pan, J. Selective Capture of Palladium(II) from Highly Acidic Solution by Proline-Valinol Amide Functionalized Silica Nanoparticles. *Colloids Surf. A Physicochem. Eng. Asp.* **2022**, *648*, 129374.
24. Chen, Y. Z.; Zhang, P.; Yang, Y.; Cao, Q.; Guo, Q. Q.; Liu, Y. S.; Chong, H. B.; Lin, M. Z. Porous g-C_3N_4 Modified with Phenanthroline Diamide for Efficient and Ultrafast Adsorption of Palladium from Simulated High Level Liquid Waste. *Environ. Sci. Nano* **2023**, *10*, 295–310.
25. Aguila, B.; Sun, Q.; Cassady, H. C.; Shan, C.; Liang, Z.; Al-Enizic, A. M.; Nafadyc, A.; Wright, J. T.; Meulenberg, R. W.; Ma, S. A Porous Organic Polymer Nanotrap for Efficient Extraction of Palladium. *Angew. Chem. Int. Ed.* **2020**, *59*, 19618–19622.
26. Nguyen, T. S.; Yavuz, C. T. Selective Palladium Recovery by a Highly Porous Polyisothiocyanurate. *Chem* **2022**, *8*, 1793–1796.
27. Wu, P. C.; Liu, H.; Sun, M. Q.; Zeng, Y. X.; Ye, J. W.; Qin, S.; Cai, Y. M.; Feng, W.; Yuan, L. H. Covalent Triazine Frameworks for the Selective Sorption of Palladium from Highly Acidic Radioactive Liquid Wastes. *J. Mater. Chem. A* **2021**, *9*, 27320–27331.
28. Li, X.; Wang, Y. L.; Wen, J.; Zheng, L.; Qian, C.; Cheng, Z.; Zuo, H.; Yu, M.; Yuan, J.; Li, R.; Zhang, W.; Liao, Y. Porous Organic Polycarbene Nanotrap for Efficient and Selective Gold Stripping from Electronic Waste. *Nat. Commun.* **2023**, *14*, 263.
29. Huang, J.; Cui, W.-R.; Wang, Y.-G.; Yan, R.-H.; Jiang, W.; Zhang, L.; Liang, R.-P.; Qiu, J.-D. Rational Designed Molecularly Imprinted Triazine-Based Porous Aromatic Frameworks for Enhanced Palladium Capture via Three Synergistic Mechanisms. *Chem. Eng. J.* **2022**, *430*, 132962.
30. Wu, X.; Lin, H., Dai, F., Hu, R., Tang, B. Functional Polyselenoureas for Selective Gold Recovery Prepared from Catalyst-Free Multicomponent Polymerizations of Elemental Selenium. *CCS Chem.* **2020**, *2*, 191–202.
31. Zha, M.; Liu, J.; Wong, Y.-L.; Xu, Z. Extraction of Palladium from Nuclear Waste-like Acidic Solutions by a Metal–Organic Framework with Sulfur and Alkene Functions. *J. Mater. Chem. A* **2015**, *3*, 3928–3934.
32. Tang, J.; Chen, Y.; Wang, S.; Kong, D.; Zhang, L. Highly Efficient Metal-Organic Frameworks Adsorbent for Pd(II) and Au(III) Recovery from Solutions: Experiment and Mechanism. *Environ. Res.* **2022**, *210*, 112870.
33. Feng, J.; Xie, M.; Xu, D. R.; Tang, Z. Z.; He, C. L.; Ning, S. Y.; Li, M.; Yuan, G. Y.; Jiang, S. S. Preparation of Metal-Organic Framework Composite Beads for Selective Adsorption and Separation of Palladium: Properties, Mechanism and Practical Application. *Sep. Purif. Technol.* **2022**, *302*, 122081.
34. Daliran, S.; Ghazagh-Miri, M.; Oveisi, A. R.; Khajeh, M.; Navalon, S.; Alvaro, M.; Ghaffari-Moghaddam, M.; Samareh Delarami, H.; Garcia, H. A Pyridyltriazol Functionalized Zirconium Metal-Organic Framework for Selective and Highly Efficient Adsorption of Palladium. *ACS Appl. Mater. Interfaces* **2020**, *12*, 25221–25232.
35. Kuo, C.-T.; Lu, Y.; Arab, P.; Weeraratne, K. S.; El-Kaderi, H.; Karim, A. M. 18.1% Single Palladium Atom Catalysts on Mesoporous Covalent Organic Framework for Gas Phase Hydrogenation of Ethylene. *Cell Rep. Phys. Sci.* **2021**, *2*, 100495.
36. Das, S.; Hazarika, G.; Manna, D. Guanidine-Functionalized Fluorescent sp^2 Carbon-Conjugated Covalent Organic Framework for Sensing and Capture of Pd(II) and Cr(VI) Ions. *Chem. Eur. J.* **2023**, *29*, e202203595.
37. Luo, J.; Luo, X.; Xie, M.; Li, H. Z.; Duan, H.; Zhou, H. G.; Wei, R. J.; Ning, G. H.; Li, D. Selective and Rapid Extraction of Trace Amount of Gold from Complex Liquids with Silver(I)-Organic Frameworks. *Nat. Commun.* **2022**, *13*, 7771.
38. Cao, S. C.; Li, D. Y.; Uliana, A. A.; Jiang, Y. L.; Zhu, J. Y.; Zhang, Y. T.; van der Bruggen, B. Multifunctional Covalent Organic Framework Membranes with an Ultrathin Recycled Palladium Nanolayer for Efficient Water Decontamination. *Appl. Catal. B* **2023**, *323*, 122175.
39. Zhao, Y. L.; Xu, C.; Qi, Q. L.; Qiu, J. K.; Li, Z. Y.; Wang, H. Y.; Wang, J. J. Tailoring Delicate Pore Environment of 2D Covalent Organic Frameworks for Selective Palladium Recovery. *Chem. Eng. J.* **2022**, *446*, 136823.
40. He, L. W.; Li, B. Y.; Ma, Z. L.; Chen, L. X.; Gong, S. C.; Zhang, M. X.; Bai, Y. Y.; Guo, Q.; Wu, F. Q.; Zhao, F. Q.; Li, J.; Zhang, D.; Sheng, D. P.; Dai, X.; Chen, L.; Shu, J.; Chai, Z. F.; Wang, S. O. Synergy of First- and Second-Sphere Interactions in a Covalent Organic Framework Boosts Highly Selective Platinum Uptake. *Sci. China Chem.* **2023**, *66*, 783–790.
41. Bai, Y.; Chen, L.; He, L.; Li, B.; Chen, L.; Wu, F.; Chen, L.; Zhang, M.; Liu, Z.; Chai, Z.; Wang, S. Precise Recognition of Palladium Through Interlaminar Chelation in a Covalent Organic Framework. *Chem* **2022**, *8*, 1442–1459.
42. Fujita, M.; Tominaga, M.; Hori, A.; Therrien, B. Coordination Assemblies from a Pd(II)-Cornered Square Complex. *Acc. Chem. Res.* **2005**, *38*, 369–378.
43. Gunn, G. Platinum-Group Metals. In *Critical Metals Handbook*; John Wiley & Sons, Ltd.: Nottingham, United Kingdom, **2014**; pp 284–311.
44. Yang, S.; Lv, H.; Zhong, H.; Yuan, D.; Wang, X.; Wang, R. Transformation of Covalent Organic Frameworks from N-Acylhydrazone to Oxadiazole Linkages for Smooth Electron Transfer in Photocatalysis. *Angew. Chem. Int. Ed.* **2022**, *61*, e202115655.
45. Li, Z.; Geng, K.; He, T.; Tan, K. T.; Huang, N.; Jiang, Q.; Nagao, Y.; Jiang, D. Editing Light Emission with Stable Crystalline Covalent Organic Frameworks via Wall Surface Perturbation. *Angew. Chem. Int. Ed.* **2021**, *60*, 19419–19427.
46. Xie, Y.; Wu, Y.; Liu, X.; Hao, M.; Chen, Z.; Waterhouse, G. I. N.; Wang, X.; Yang, H.; Ma, S. Rational Design of Cooperative Chelating Sites on Covalent Organic Frameworks for Highly Selective Uranium Extraction from Seawater. *Cell Rep. Phys. Sci.* **2023**, *4*, 101220.

DOI: 10.31635/ccschem.023.202303404
Citation: *CCS Chem.* **2024**, 6, 1908–1919
Link to VoR: https://doi.org/10.31635/ccschem.023.202303404

47. Li, Y.; Sui, J.; Cui, L. S.; Jiang, H. L. Hydrogen Bonding Regulated Flexibility and Disorder in Hydrazone-Linked Covalent Organic Frameworks. *J. Am. Chem. Soc.* **2023**, *145*, 1359–1366.
48. Li, X.; Gao, Q.; Wang, J.; Chen, Y.; Chen, Z. H.; Xu, H. S.; Tang, W.; Leng, K.; Ning, G. H.; Wu, J.; Xu, Q. H.; Quek, S. Y.; Lu, Y.; Loh, K. P. Tuneable Near White-Emissive Two-Dimensional Covalent Organic Frameworks. *Nat. Commun.* **2018**, *9*, 2335.
49. Qian, C.; Zhou, W.; Qiao, J.; Wang, D.; Li, X.; Teo, W. L.; Shi, X.; Wu, H.; Di, J.; Wang, H.; Liu, G.; Gu, L.; Liu, J.; Feng, L.; Liu, Y.; Quek, S. Y.; Loh, K. P.; Zhao, Y. Linkage Engineering by Harnessing Supramolecular Interactions to Fabricate 2D Hydrazone-Linked Covalent Organic Framework Platforms Toward Advanced Catalysis. *J. Am. Chem. Soc.* **2020**, *142*, 18138–18149.
50. Li, X.; Qiao, J. S.; Chee, S. W.; Xu, H. S.; Zhao, X. X.; Choi, H. S.; Yu, W.; Quek, S. Y.; Mirsaidov, U.; Loh, K. P. Rapid, Scalable Construction of Highly Crystalline Acylhydrazone Two-Dimensional Covalent Organic Frameworks via Dipole-Induced Antiparallel Stacking. *J. Am. Chem. Soc.* **2020**, *142*, 4932–4943.
51. Peng, L.; Zhang, M.; Dong, Z.; Qi, W.; Zhai, M.; Zhao, L. Efficient and Selective Adsorption of Pd(II) by Amino Acid-Functionalized Cellulose Microspheres and Their Applications in Palladium Recovery from PCBs Leaching Solution. *Sep. Purif. Technol.* **2022**, *301*, 122037.
52. Tang, Z.; Xu, D.; Chen, H.; Tang, S.; He, C.; Ning, S.; Li, M.; Yuan, G.; Chen, S.; Feng, J. Adsorption of Pd(II) from Wastewater by a Functionalized Metal-Organic Framework with Aminopyridine Structure: Performance and Mechanism. *Micropor. Mesopor. Mater.* **2023**, *353*, 122519.
53. Wu, F.; Li, H.; Pan, Y.; Sun, Y.; Pan, J. Bioinspired Construction of Magnetic Nano Stirring Rods with Radially Aligned Dual Mesopores and Intrinsic Rapid Adsorption of Palladium. *J. Hazard. Mater.* **2023**, *441*, 129917.
54. Zhang, K.; Chang, Z.; Luo, X.; Yang, L.; Pei, J.; Luo, S. Specific Spatial Transfer $PdCl_4^{2-}$ to [X-Pd-Y] by Strong Coordination Interaction in a 3D Palladium Ion-Imprinted Polymer with Footprint Cavity. *Chem. Eng. J.* **2021**, *405*, 126613.
55. Chen, G.; Wang, Y.; Weng, H.; Wu, Z.; He, K.; Zhang, P.; Guo, Z.; Lin, M. Selective Separation of Pd(II) on Pyridine-Functionalized Graphene Oxide Prepared by Radiation-Induced Simultaneous Grafting Polymerization and Reduction. *ACS Appl. Mater. Interfaces* **2019**, *11*, 24560–24570.
56. Hao, M.; Chen, Z.; Liu, X.; Liu, X.; Zhang, J.; Yang, H.; Waterhouse, G. I. N.; Wang, X.; Ma, S. Converging Cooperative Functions into the Nanospace of Covalent Organic Frameworks for Efficient Uranium Extraction from Seawater. *CCS Chem.* **2022**, *4*, 2294–2307.

DOI: 10.31635/ccschem.023.202303404
Citation: *CCS Chem.* **2024**, 6, 1908–1919
Link to VoR: https://doi.org/10.31635/ccschem.023.202303404